AIMS Mathematics, 11(1): 1202–1218.
DOI: 10.3934/math.2026051
Received: 29 September 2025
Revised: 27 December 2025
Accepted: 06 January 2026
Published: 16 January 2026

http://www.aimspress.com/journal/Math

Research article

Resonant peak tuning of a nonlinear multi-mode perforated panel absorber by pre-setting its deflection profile

Kongzheng Liang[1], Di Zeng[2], Yiuyin Lee[3,*] and Zongxian Wang[1]

[1] Institute of Systems Science, Beijing Wuzi University, Beijing 101149, China
[2] Institute of Acoustics, Chinese Academy of Sciences, Beijing, 100190, China
[3] Department of Architecture and Civil Engineering, City University of Hong Kong, Kowloon Tong, Kowloon, Hong Kong

* **Correspondence:** Email: bcraylee@cityu.edu.hk.

Abstract: In this paper, we addressed the absorption of sound by a nonlinear multi-mode panel absorber. Nonlinear structural vibration has been greatly investigated in recent decades, but very few researchers have considered structural nonlinearities in structural–acoustic models. Importantly, the first structural resonant frequency of a perforated panel absorber with typical dimensions is much lower than the absorption peak frequency. The results of this study indicated that such resonant vibration cannot enhance the absorption performance. Thus, a novel approach was proposed, namely to increase the first nonlinear panel resonant frequency by pre-setting the initial deflection profile, enabling the resonant vibration effect to be used for widening the absorption bandwidth. A new solution method, termed the phase angle elimination method, was developed for cases of damped nonlinear vibration. The principle of the method was to transform the nonlinear governing equation of a perforated panel into a set of multi-mode formulations. A numerical case study was conducted to examine the effects of various parameters on the absorption performance.

Keywords: panel absorber; noise and vibration; sound absorption; acoustics
Mathematics Subject Classification: 37M05, 65M99, 65P99

1. Introduction

In this paper, we present an innovative sound-absorption technique and a classical solution

method for the resulting governing equations. The innovative technique involves increasing the panel resonant frequency of an absorber by pre-setting the initial deflection profile to widen the absorption bandwidth. The method of solving the nonlinear governing equation, termed the phase angle elimination method, involves eliminating the phase angles by squaring and adding the nonlinear equations generated in the harmonic balance process. The conventional linear damping assumption is adopted in the modeling procedure. To calculate the absorption coefficient, the impedances of the structural and acoustic items are obtained and combined.

Tunable acoustic metamaterials, nonlinear panel vibration, linear sound absorption, and vibration have attracted widespread research interest. Most researchers investigating the areas of structural dynamics and acoustics have focused on theoretical modeling and solution method development without any experimentation. For example, Hu et al. [1] presented a modeling and dynamic analysis on spar-type floating offshore wind turbines system via structure-preserving iterative method. They developed a coupled dynamic model based on the Hamilton's variational principle and generalized multi-symplectic method. The dynamic responses of the spar-type floating offshore wind turbines system were studied for various wind field cases. Xi et al. [2] studied a hub-cracked beam with hollow tapered cross-section using a structure-preserving method. An iteration approach was used to develop a coupled dynamic model for the planar rotation and the transverse vibration of the system. The effects of the crack's parameters on the various stabilities were examined in the numerical simulations. The accuracy of the proposed method was also verified by a finite element method. Hu et al. [3] investigated the coupling dynamic behaviors of flexible thin-walled tapered hub-beam with a tip mass. The governing equations representing the coupling system were developed. Then, the formulations with dynamic symmetry-breaking factor were obtained for the vibration of the system using the Preissmann scheme. From the results, the contour lines of the stable vibration amplitude showed the important effects of the tip mass on the dynamic responses. Kan et al. [4] reproduced the vibration localization in a mistuned bladed disk system. They considered the morphological characteristics and the micro-dynamic behaviors to establish an improved dry friction model to study the coupling effects and the dynamic responses of the entire bladed disk system. In the numerical results, the phenomenon of vibration localization was generated and various influences were revealed. Some have focused solely on either the nonlinear vibrational responses or the acoustic properties, without addressing both. Chen et al.'s [5] review highlighted advances in the technology of tunable acoustic metamaterials based on modulation techniques. Such techniques are principally developed to extend the acoustic response into wider frequency bands, creating tunable acoustic metamaterials capable of good acoustic performance for specific applications. These and other technologies for improving acoustic performance (e.g., mechanical loading, magnetic control, and active control) are based on very different principles from those that exploit nonlinear/large-deflection vibration phenomena, which usually do not require additional devices or special materials (e.g., magnetic control/active control systems, damping materials, and metamaterials). In this study, a technique based on tuning the structural properties of a conventional material to induce nonlinear phenomena is developed, aiming to improve the acoustic performance. Pandey et al. [6] presented a thermoelastic stability analysis of laminated composite plates. Higher-order shear deformation theory and von-Karman nonlinear kinematics were adopted in developing the mathematical formulations of the problem, which exhibited cubic nonlinearity owing to the shear deformable elastic foundation. The nonlinear governing equations were solved by a two-part procedure: First using the quadratic extrapolation technique for linearization, then using the fast-converging finite double Chebyshev series for spatial discretization. The effects of various parameters

on the buckling and postbuckling responses were studied. Li and Yao [7] proposed a double-mode model representing the nonlinear flexural vibration of a sandwiched thin panel with a symmetric rectangular honeycomb geometry. The Galerkin method and homotopy analysis were used to derive and solve the two major coupled nonlinear governing equations, and the primary and harmonic resonances were analyzed. The proposed method was used to identify the softening and hardening nonlinear characteristics. Shahmohammadi et al. [8] addressed the geometrically nonlinear and size-dependent responses of shallow, sandwiched, curved micro-panels. The governing equations were obtained using a modified first-order shear deformation theory and the Galerkin method. The effects of mechanical and geometrical properties on the forced vibrations were investigated. Zheng et al. [9] analyzed the acoustic characteristics of an ultra-micro-perforated panel absorber under oblique incidence using finite element simulations and discrete integral calculations. It was found that the sound absorption was optimized in the case of 45-degree incidence. The proposed absorber achieved an average absorption coefficient of 0.9 across the medium to high frequency range. Lee et al. [10] conducted a theoretical and experimental analysis of a finite flexible micro-perforated panel absorber. Absorption was optimized by appropriately selecting the perforation and structural parameters based on a parametric analysis. The absorption bandwidth was found to widen when the linear structural resonant frequency was set higher than the absorption peak frequency caused by the perforations.

Nonlinear structural acoustics has been relatively rarely studied. Lee [11] presented a study of absorption by a flat panel absorber under the influence of perforation, air pumping, and nonlinear vibration. A simple single-mode approach was adopted to develop a concise absorption formula. This study differs from that of Lee [11] in several respects, including the pre-set deflection profile and solution method. Lee et al. [12] theoretically and experimentally investigated the sound absorption of a nonlinearly vibrating curved panel. The theoretical formulation was developed based on the assumptions of quadratic and cubic nonlinear structural vibrations, linear damping, and linear acoustics. Indeed, most structural or acoustic models have employed linear damping assumptions (e.g., [13]). The reported theoretical and experimental observations have generally been in agreement. Some discrepancies around the resonant peaks and resonant frequency shifts have been observed, attributed to the assumptions of linear damping and ideal boundary conditions. Zhou et al. [14] used a nonlinear vibration absorber to suppress the nonlinear response of a panel flutter in supersonic airflow. The nonlinear aero-elastic equations of a three-dimensional panel were established using Galerkin's method and piston aerodynamic theory. The results showed that the nonlinear aero-elastic responses of the panel were significantly reduced by recurrent transient resonance capture and permanent resonance capture in the suppression region. As mentioned, few researchers have incorporated structural nonlinearity into their vibro-acoustic models, and those that have done so focused on very specific problems unrelated to that in this paper.

2. Theoretical formulation

Consider a panel with a pre-static deflection profile backed by a cavity (see Figure 1). Before obtaining the absorption coefficient, the panel impedance is derived using the phase angle elimination method. Then, the cavity and perforation impedances are considered and combined with the panel impedance using the electro-acoustic analogy. The governing equation of the panel with a pre-static deflection profile is given by [12].

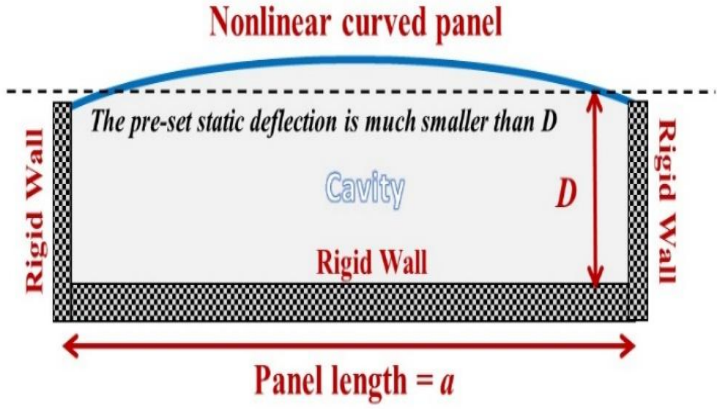

Figure 1. A panel with a pre-static deflection profile backed by a cavity.

$$\rho\frac{\mathrm{d}^2y}{\mathrm{d}t^2}+EI\frac{\mathrm{d}^4y}{\mathrm{d}x^4}-\frac{Ebh}{a}\frac{\mathrm{d}^2(y+y_o)}{\mathrm{d}x^2}\int_0^a\left(\frac{\mathrm{d}y}{\mathrm{d}x}\frac{\mathrm{d}y_o}{\mathrm{d}x}+\frac{1}{2}\left(\frac{\mathrm{d}y_o}{\mathrm{d}x}\right)^2\right)dx=F(t), \tag{1}$$

where ρ is the panel density per unit length; E is Young's modulus; I is the second moment of area; y_o is the initial deflection profile (i.e., $A_o\sin\left(\frac{\pi}{a}x\right)$), A_o is the initial center deflection); a, b, and h are the panel length, width, and thickness, respectively; $F(t)=\kappa\rho g\cos(\omega t)$; κ is a dimensionless excitation parameter; ω is the excitation frequency; g is gravity; and y is the transverse displacement, which can be expressed in the following form

$$y(x,t)=A_1\sin\left(\frac{\pi}{a}x\right)+A_3\sin\left(\frac{3\pi}{a}x\right)+A_5\sin\left(\frac{5\pi}{a}x\right)... \tag{2}$$

In Eq (1), the nonlinear modal coupling terms come from $\frac{\mathrm{d}^2(y+y_o)}{\mathrm{d}x^2}\int_0^a\left(\frac{\mathrm{d}y}{\mathrm{d}x}\frac{\mathrm{d}y_o}{\mathrm{d}x}\right)dx$, which represents the nonlinear structural stiffness. It can be seen that if the pre-set deflection y_o is increased, then the nonlinear modal coupling effects between A_1, A_3, and A_5 in Eq (2) will also increase. In this study, a three-mode approach is adopted. The corresponding modal equations are derived (in the next section, it is proven that this three-mode approach is accurate enough). The first modal reduction process involves multiplying $\sin\left(\frac{\pi}{a}x\right)$ by each side of Eq (1) and integrating with respect to x.

$$\begin{aligned}&\frac{1}{2}\rho a\frac{\mathrm{d}^2A_1}{\mathrm{d}t^2}+\left(\frac{\pi^4}{2}\frac{EI}{a^3}+\frac{\pi^2}{4}\frac{Ebh}{a^3}(A_0)^2\right)A_1+\qquad\frac{\pi^4}{8}\frac{Ebh}{a^3}[(A_1)^3+9A_1(A_3)^2+25A_1(A_5)^2+\\&3A_o(A_1)^2+9A_o(A_3)^2+25A_o(A_5)^2]=\kappa\frac{2\rho ag}{\pi}\cos(\omega t)\\&\Rightarrow\\&\frac{\mathrm{d}^2A_1}{\mathrm{d}t^2}+(\omega_1)^2A_1+\beta_1[(A_1)^3+9A_1(A_3)^2+25A_1(A_5)^2+3A_o(A_1)^2+9A_o(A_3)^2+\end{aligned} \tag{3}$$

$25A_o(A_5)^2] = \kappa\frac{4g}{\pi}\cos(\omega t)$,

where $\omega_1 = \frac{\pi^2}{a^2}\sqrt{\frac{EI}{\rho}\left(1+\frac{bh}{2I\pi^2}(A_0)^2\right)}$; $\beta_1 = \frac{Ebh\pi^4}{4\rho a^4}$.

Again, multiply $\sin\left(\frac{3\pi}{a}x\right)$ by each side of Eq (1) and integrate with respect to *x*.

$$\frac{1}{2}\rho a\frac{d^2A_3}{dt^2} + \left(\frac{(3\pi)^4}{2}\frac{EI}{a^3}\right)A_3 + \frac{9\pi^4}{8}\frac{Ebh}{a^3}\left[2A_0A_1A_3 + A_3(A_1)^2 + 25A_3(A_5)^2 + 9{A_3}^3\right] = \kappa\frac{2\rho ag}{3\pi}\cos(\omega t)$$

$$\Rightarrow \tag{4}$$

$$\frac{d^2A_3}{dt^2} + (\omega_3)^2A_3 + \beta_3\left[2A_0A_1A_3 + A_3(A_1)^2 + 25A_3(A_5)^2 + 9{A_3}^3\right] = \kappa\frac{4g}{3\pi}\cos(\omega t),$$

where $\omega_3 = \frac{(3\pi)^2}{a^2}\sqrt{\frac{EI}{\rho}}$; $\beta_3 = \frac{9}{4}\frac{Ebh\pi^4}{\rho a^4}$.

Again, multiply $\sin\left(\frac{5\pi}{a}x\right)$ by each side of Eq (1) and integrate with respect to *x*

$$\frac{1}{2}\rho a\frac{d^2A_5}{dt^2} + \frac{1}{2}(5\pi)^4\frac{EI}{a^3}A_5 + \frac{25\pi^4}{8}\frac{Ebh}{a^3}[2A_0A_1A_5 + A_5(A_1)^2 + 9A_5(A_3)^2 + 25(A_5)^3] = \kappa\frac{2\rho ag}{5\pi}\cos(\omega t)$$

$$\Rightarrow \tag{5}$$

$$\frac{d^2A_5}{dt^2} + (\omega_5)^2A_5 + \beta_5[2A_0A_1A_5 + A_5(A_1)^2 + 9A_5(A_3)^2 + 25(A_5)^3] = \kappa\frac{4\rho ag}{5\pi}\cos(\omega t)$$

where $\omega_5 = \frac{(5\pi)^2}{a^2}\sqrt{\frac{EI}{\rho}}$; $\beta_5 = \frac{25}{4}\frac{Ebh\pi^4}{\rho a^4}$.

Add a damping term into the first modal governing equation to obtain the following equation:

$$\frac{d^2A_1}{dt^2} + (\omega_1)^2A_1 + \xi\omega_1\frac{dA_1}{dt} + \beta_1[(A_1)^3 + 9A_1(A_3)^2 + 3A_o(A_1)^2 + 9A_o(A_3)^2] = \kappa\frac{4g}{\pi}\cos(\omega t), \tag{6}$$

where ξ is the linear damping ratio.

Consider two harmonic terms in the following approximation form:

$$A_1(t) = A_{11}\cos(\omega t + \theta) + A_{13}\cos(3\omega t + 3\theta) \tag{7}$$

Insert (7) into (6) and perform the harmonic balance of $\cos(\omega t)$.

$$\begin{aligned}&(-\omega^2 + (\omega_1)^2)A_{11}\cos(\theta) - \xi\omega_1\omega A_{11}\sin(\theta) + \\ &\frac{1}{4}\beta_1[3(A_{11})^3 + 3A_{13}(A_{11})^2 \\ &\quad + (50(A_{53})^2 + 50A_{51}A_{53} + 75(A_{51})^2 + 27(A_{31})^2 + 6(A_{13})^2 + 18(A_{33})^2 \\ &\quad + 18A_{13}A_{33})A_{11} + 12A_{13}A_{31}A_{33} + 3A_{13}(A_{31})^2]\cos(\theta) = \kappa\frac{4g}{\pi}.\end{aligned} \tag{8}$$

Insert (7) into (6) and perform the harmonic balance of $\sin(\omega t)$:

$$(-\omega^2+(\omega_1)^2)A_{11}\sin(\theta)+\xi\omega_1\omega A_{11}\cos(\theta)+$$
$$\frac{1}{4}\beta_1[3(A_{11})^3+3A_{13}(A_{11})^2$$
$$+(50(A_{53})^2+50A_{51}A_{53}+75(A_{51})^2+27(A_{31})^2+6(A_{13})^2+18(A_{33})^2$$
$$+18A_{13}A_{33})A_{11}+12A_{13}A_{31}A_{33}+3A_{13}(A_{31})^2]\sin(\theta)=0. \quad (9)$$

The phase angle can be eliminated by squaring both sides of (8-9) and adding them together. Then, the $\sin(\theta)$ and $\cos(\theta)$ terms can be eliminated.

$$\left\{(-\omega^2+(\omega_1)^2)A_{11}+\frac{1}{4}\beta_1[3(A_{11})^3+3A_{13}(A_{11})^2+(50(A_{53})^2+50A_{51}A_{53}+\right.$$
$$75(A_{51})^2+27(A_{31})^2+6(A_{13})^2+18(A_{33})^2+18A_{13}A_{33})A_{11}+12A_{13}A_{31}A_{33}+ \quad (10)$$
$$\left.3A_{13}(A_{31})^2]\right\}^2+\{\xi\omega_1\omega A_{11}\}^2=\left\{\kappa\frac{4g}{\pi}\right\}^2.$$

Insert (7) into (6) and perform the harmonic balance of $\cos(3\omega t)$.

$$(-9\omega^2+(\omega_1)^2)A_{13}\cos(3\theta)-3\xi\omega_1\omega A_{13}\sin(3\theta)+$$
$$\frac{1}{4}\beta_1[(A_{11})^3+6A_{13}(A_{11})^2+(36A_{31}A_{33}+9(A_{31})^2+25(A_{51})^2+100A_{51}A_{53})A_{11}+ \quad (11)$$
$$27A_{13}(A_{33})^2+3(A_{13})^3+50A_{13}(A_{51})^2+18A_{13}(A_{31})^2+75A_{13}(A_{53})^2]\cos(3\theta)=0.$$

Insert (7) into (6) and perform the harmonic balance of $\sin(3\omega t)$.

$$(-9\omega^2+(\omega_1)^2)A_{13}\sin(3\theta)+3\xi\omega_1\omega A_{13}\cos(3\theta)+$$
$$\frac{1}{4}\beta_1[(A_{11})^3+6A_{13}(A_{11})^2+(36A_{31}A_{33}+9(A_{31})^2+25(A_{51})^2+100A_{51}A_{53})A_{11}+ \quad (12)$$
$$27A_{13}(A_{33})^2+3(A_{13})^3+50A_{13}(A_{51})^2+18A_{13}(A_{31})^2+75A_{13}(A_{53})^2]\sin(3\theta)=0.$$

Again, the phase angle can be eliminated by squaring both sides of (11-12) and adding them together. The $\sin(3\theta)$ and $\cos(3\theta)$ terms can be eliminated.

$$\left\{(-9\omega^2+(\omega_1)^2)A_{13}+\frac{1}{4}\beta_1[(A_{11})^3+6A_{13}(A_{11})^2+(36A_{31}A_{33}+9(A_{31})^2+25(A_{51})^2+\right.$$
$$100A_{51}A_{53})A_{11}+27A_{13}(A_{33})^2+3(A_{13})^3+50A_{13}(A_{51})^2+18A_{13}(A_{31})^2+ \quad (13)$$
$$\left.75A_{13}(A_{53})^2]\right\}^2+\{3\xi\omega_1\omega A_{13}\}^2=0.$$

Add a damping term in the second modal governing equation to obtain the following equation:

$$\frac{\mathrm{d}^2A_3}{\mathrm{d}t^2}+(\omega_3)^2A_3+\xi\omega_3\frac{dA_3}{\mathrm{d}t}+\beta_3\left[2A_0A_1A_3+A_3(A_1)^2+25A_3(A_5)^2+9{A_3}^3\right]=\kappa\frac{4g}{3\pi}\cos(\omega t). \quad (14)$$

Consider two harmonic terms in the following approximation form:

$$A_3(t)=A_{31}\cos(\omega t+\theta)+A_{33}\cos(3\omega t+3\theta). \quad (15)$$

Insert (15) into (14) and perform the harmonic balance of $\cos(\omega t)$.

$$(-\omega^2+(\omega_3)^2)A_{31}\cos(\theta)-\xi\omega_3\omega A_{31}\sin(\theta)+\frac{1}{4}\beta_3[27(A_{31})^3+27A_{33}(A_{31})^2+ \quad (16)$$

$$(3(A_{11})^2 + 50(A_{53})^2 + 2A_{11}A_{13} + 54(A_{33})^2 + 2(A_{13})^2 + 50A_{51}A_{53} + 75(A_{51})^2)A_{31} + A_{33}(A_{11})^2 + 25A_{33}(A_{51})^2 + 100A_{33}A_{51}A_{53} + 4A_{11}A_{13}A_{33}]\cos(\theta) = \kappa\frac{4g}{3\pi}.$$

Insert (15) into (14) and perform the harmonic balance of $\sin(\omega t)$.

$$\begin{aligned}&(-\omega^2 + (\omega_3)^2)A_{31}\sin(\theta) + \xi\omega_3\omega A_{31}\cos(\theta) + \\ &\frac{1}{4}\beta_3[27(A_{31})^3 + 27A_{33}(A_{31})^2 + (3(A_{11})^2 + 50(A_{53})^2 + 2A_{11}A_{13} + 54(A_{33})^2 + \\ &2(A_{13})^2 + 50A_{51}A_{53} + 75(A_{51})^2)A_{31} + A_{33}(A_{11})^2 + 25A_{33}(A_{51})^2 + 100A_{33}A_{51}A_{53} + \\ &4A_{11}A_{13}A_{33}]\sin(\theta) = 0.\end{aligned} \tag{17}$$

The phase angle can be eliminated by squaring both sides of (16-17) and adding them together. The $\sin(\theta)$ and $\cos(\theta)$ terms can be eliminated.

$$\begin{aligned}&\left\{(-\omega^2 + (\omega_3)^2)A_{31} + \frac{1}{4}\beta_3[27(A_{31})^3 + 27A_{33}(A_{31})^2 + (3(A_{11})^2 + 50(A_{53})^2 + \right. \\ &2A_{11}A_{13} + 54(A_{33})^2 + 2(A_{13})^2 + 50A_{51}A_{53} + 75(A_{51})^2)A_{31} + A_{33}(A_{11})^2 + \\ &\left.25A_{33}(A_{51})^2 + 100A_{33}A_{51}A_{53} + 4A_{11}A_{13}A_{33}]\right\}^2 + \{\xi\omega_3\omega A_{31}\}^2 = \left\{\kappa\frac{4g}{3\pi}\right\}^2.\end{aligned} \tag{18}$$

Insert (15) into (14) and perform the harmonic balance of $\cos(3\omega t)$.

$$\begin{aligned}&(-9\omega^2 + (\omega_3)^2)A_{33}\cos(3\theta) - 3\xi\omega_3\omega A_{33}\sin(3\theta) + \\ &\frac{1}{4}\beta_3[9(A_{31})^3 + 54A_{33}(A_{31})^2 + (4A_{11}A_{13} + 25(A_{51})^2 + (A_{11})^2 + 100A_{51}A_{53})A_{31} + \\ &3A_{33}(A_{13})^2 + 2A_{33}(A_{11})^2 + 27(A_{33})^3 + 75A_{33}(A_{53})^2 + 50A_{33}(A_{51})^2]\cos(3\theta) = 0.\end{aligned} \tag{19}$$

Insert (15) into (14) and perform the harmonic balance of $\sin(3\omega t)$.

$$\begin{aligned}&(-9\omega^2 + (\omega_3)^2)A_{33}\sin(3\theta) + 3\xi\omega_3\omega A_{33}\cos(3\theta) + \\ &\frac{1}{4}\beta_3[9(A_{31})^3 + 54A_{33}(A_{31})^2 + (4A_{11}A_{13} + 25(A_{51})^2 + (A_{11})^2 + 100A_{51}A_{53})A_{31} + \\ &3A_{33}(A_{13})^2 + 2A_{33}(A_{11})^2 + 27(A_{33})^3 + 75A_{33}(A_{53})^2 + 50A_{33}(A_{51})^2]\sin(3\theta) = 0.\end{aligned} \tag{20}$$

The phase angle elimination process can be done by squaring both sides of (19-20) and adding them together. The $\sin(3\theta)$ and $\cos(3\theta)$ terms can be eliminated.

$$\begin{aligned}&\left\{(-9\omega^2 + (\omega_3)^2)A_{33} + \frac{1}{4}\beta_3[9(A_{31})^3 + 54A_{33}(A_{31})^2 + (4A_{11}A_{13} + 25(A_{51})^2 + (A_{11})^2 + \right. \\ &100A_{51}A_{53})A_{31} + 3A_{33}(A_{13})^2 + 2A_{33}(A_{11})^2 + 27(A_{33})^3 + 75A_{33}(A_{53})^2 + \\ &\left.50A_{33}(A_{51})^2]\right\}^2 + \{3\xi\omega_3\omega A_{33}\}^2 = 0.\end{aligned} \tag{21}$$

Add a damping term in the third modal governing equation to obtain the following equation:

$$\frac{\mathrm{d}^2A_5}{\mathrm{d}t^2} + (\omega_5)^2A_5 + \xi\omega_5\frac{dA_5}{\mathrm{d}t} + \beta_5[2A_0A_1A_5 + A_5(A_1)^2 + 9A_5(A_3)^2 + 25(A_5)^3] = \kappa\frac{4\rho ag}{5\pi}\cos(\omega t). \tag{22}$$

Consider two harmonic terms in the following approximation form:

$$A_5(t) = A_{51}\cos(\omega t + \theta) + A_{53}\cos(3\omega t + 3\theta). \tag{23}$$

Insert (23) into (22) and perform the harmonic balance of $\cos(\omega t)$

$$\begin{aligned}&(-\omega^2 + (\omega_5)^2)A_{51}\cos(\theta) - \xi\omega_5\omega A_{51}\sin(\theta) + \\ &\frac{1}{4}\beta_5[75(A_{51})^3 + 75A_{53}(A_{51})^2 + (18(A_{33})^2 + 150(A_{53})^2 + 3(A_{11})^2 + 18A_{31}A_{33} + \\ &2A_{11}A_{13} + 27(A_{31})^2 + 2(A_{13})^2)A_{51} + 36A_{53}A_{31}A_{33} + A_{53}(A_{11})^2 + 4A_{53}A_{11}A_{13} + \\ &9A_{53}(A_{31})^2]\cos(\theta) = \kappa\frac{4g}{5\pi}.\end{aligned} \tag{24}$$

Insert (23) into (22) and perform the harmonic balance of $\sin(\omega t)$

$$\begin{aligned}&(-\omega^2 + (\omega_5)^2)A_{51}\sin(\theta) + \xi\omega_5\omega A_{51}\cos(\theta) + \\ &\frac{1}{4}\beta_5[75(A_{51})^3 + 75A_{53}(A_{51})^2 + (18(A_{33})^2 + 150(A_{53})^2 + 3(A_{11})^2 + 18A_{31}A_{33} + \\ &2A_{11}A_{13} + 27(A_{31})^2 + 2(A_{13})^2)A_{51} + 36A_{53}A_{31}A_{33} + A_{53}(A_{11})^2 + 4A_{53}A_{11}A_{13} + \\ &9A_{53}(A_{31})^2]\sin(\theta) = 0.\end{aligned} \tag{25}$$

The phase angle can be eliminated by squaring both sides of (24-25) and adding them together. The $\sin(\theta)$ and $\cos(\theta)$ terms can be eliminated.

$$\begin{aligned}&\Big\{(-\omega^2 + (\omega_5)^2)A_{51} \\ &\qquad + \frac{1}{4}\beta_5[75(A_{51})^3 + 75A_{53}(A_{51})^2 \\ &\qquad + (18(A_{33})^2 + 150(A_{53})^2 + 3(A_{11})^2 + 18A_{31}A_{33} + 2A_{11}A_{13} + 27(A_{31})^2 \\ &\qquad + 2(A_{13})^2)A_{51} + 36A_{53}A_{31}A_{33} + A_{53}(A_{11})^2 + 4A_{53}A_{11}A_{13} \\ &\qquad + 9A_{53}(A_{31})^2]\Big\}^2 + \{\xi\omega_5\omega A_{51}\}^2 = \left\{\kappa\frac{4g}{5\pi}\right\}^2.\end{aligned} \tag{26}$$

Insert (23) into (22) and perform the harmonic balance of $\cos(3\omega t)$.

$$\begin{aligned}&(-9\omega^2 + (\omega_5)^2)A_{53}\cos(3\theta) - 3\xi\omega_5\omega A_{53}\sin(3\theta) + \frac{1}{4}\beta_5[25(A_{51})^3 + 150A_{53}(A_{51})^2 + \\ &(4A_{11}A_{13} + 36A_{31}A_{33} + (A_{11})^2 + 9(A_{31})^2)A_{51} + 18A_{53}(A_{31})^2 + 27A_{53}(A_{33})^2 + \\ &2A_{53}(A_{11})^2 + 3A_{53}(A_{13})^2 + 75(A_{53})^3]\cos(\theta) = 0.\end{aligned} \tag{27}$$

Insert (23) into (22) and perform the harmonic balance of $\sin(3\omega t)$

$$\begin{aligned}&(-9\omega^2 + (\omega_5)^2)A_{53}\sin(3\theta) + 3\xi\omega_5\omega A_{53}\cos(3\theta) \\ &+ \frac{1}{4}\beta_5[25(A_{51})^3 + 150A_{53}(A_{51})^2 + (4A_{11}A_{13} + 36A_{31}A_{33} + (A_{11})^2 + 9(A_{31})^2)A_{51} +\end{aligned} \tag{28}$$

$$18A_{53}(A_{31})^2 + 27A_{53}(A_{33})^2 + 2A_{53}(A_{11})^2 + 3A_{53}(A_{13})^2 + 75(A_{53})^3]\sin(3\theta) = 0.$$

The phase angle can be eliminated by squaring both sides of (27-28) and adding them together. The $\sin(3\theta)$ and $\cos(3\theta)$ terms can be eliminated.

$$\begin{aligned}\Big\{&(-9\omega^2 + (\omega_5)^2)A_{53} \\ &+ \frac{1}{4}\beta_5[25(A_{51})^3 + 150A_{53}(A_{51})^2 \\ &+ (4A_{11}A_{13} + 36A_{31}A_{33} + (A_{11})^2 + 9(A_{31})^2)A_{51} + 18A_{53}(A_{31})^2 \\ &+ 27A_{53}(A_{33})^2 + 2A_{53}(A_{11})^2 + 3A_{53}(A_{13})^2 + 75(A_{53})^3]\Big\}^2 + \{3\xi\omega_5\omega A_{53}\}^2 \\ &= 0.\end{aligned} \tag{29}$$

From the above procedures, the six unknowns (i.e., $A_{11}, A_{13}, A_{33}, A_{35}, A_{51}$, and A_{53}) can be found by solving the six equations (i.e., (10), (13), (18), (21), (26), and (29)). Note that if the classical harmonic balance method are used, there would be twelve equations generated because twelve unknowns are set in the solution form (see the following solution forms in the classical harmonic method)

$$\begin{aligned}y(x,t) = &(A_{11}\sin(\omega t) + A_{13}\sin(3\omega t) + B_{11}\cos(\omega t) + B_{13}\cos(3\omega t))\sin\left(\frac{\pi}{a}x\right) \\ &+(A_{31}\sin(\omega t) + A_{33}\sin(3\omega t) + B_{31}\cos(\omega t) + B_{33}\cos(3\omega t))\sin\left(\frac{3\pi}{a}x\right) \\ &+(A_{51}\sin(\omega t) + A_{53}\sin(3\omega t) + B_{51}\cos(\omega t) + B_{53}\cos(3\omega t))\sin\left(\frac{5\pi}{a}x\right),\end{aligned} \tag{30}$$

where $A_{11}, A_{13}, A_{33}, A_{35}, A_{51}, and\ A_{53}$ and $B_{11}, B_{13}, B_{33}, B_{35}, B_{51},\ and\ B_{53}$ are the unknowns for corresponding sine and cosine components. Hence, the advantage of the phase angle elimination is that a smaller number of nonlinear equations are generated in the solution procedures. Due to the difference between the solution forms of the phase angle elimination and classical harmonic balance methods, the resonant peak values obtained from these two methods would deviate from each other in nonlinear cases.

Then, the normalized modal impedances of the panel are given by

$$Z_1 = \frac{\rho'\xi\omega_1\omega - j\left[\rho'(-\omega^2 + (\omega_1)^2) + \frac{3}{4}\beta'_1(\bar{A}_1)^2\right]}{\rho_a C_a\ \omega}, \tag{31}$$

$$Z_3 = \frac{\rho'\xi\omega_3\omega - j\left[\rho'(-\omega^2 + (\omega_3)^2) + \frac{3}{4}\beta'_3(3\bar{A}_3)^2\right]}{\rho_a C_a\ \omega}, \tag{32}$$

$$Z_5 = \frac{\rho'\xi\omega_5\omega - j\left[\rho'(-\omega^2 + (\omega_5)^2) + \frac{3}{4}\beta'_5(5\bar{A}_5)^2\right]}{\rho_a C_a \omega}. \tag{33}$$

where $\bar{A}_1 = A_{11} + A_{13}$; $\bar{A}_3 = A_{31} + A_{33}$; and $\bar{A}_5 = A_{51} + A_{53}$. $\beta'_1 = \beta_1\rho'$; $\beta'_3 = \beta_3\rho'$; $\beta'_5 =$

$\beta_5\rho'$; ρ' is the panel density per unit area; ρ_a is the air density; and C_a is the sound speed.

Consider the overall panel velocity contributed by the modal velocities and find the overall panel impedance.

$$V_p = F_o\left(\frac{\Lambda_1}{Z_1}+\frac{\Lambda_3}{Z_3}+\frac{\Lambda_5}{Z_5}\right) \Rightarrow Z_p = \frac{F_o}{V_p} = \frac{1}{\left(\frac{\Lambda_1}{Z_1}+\frac{\Lambda_3}{Z_3}+\frac{\Lambda_5}{Z_5}\right)}, \tag{34}$$

where $\Lambda_1 = \frac{4\sqrt{2}}{\pi^2}$; $\Lambda_3 = \frac{4\sqrt{2}}{9\pi^2}$; $\Lambda_5 = \frac{4\sqrt{2}}{25\pi^2}$; $F_1 = \kappa\frac{4g}{\pi}$; $F_3 = \kappa\frac{4g}{3\pi}$; $F_5 = \kappa\frac{4g}{5\pi}$; $F_o = \kappa g$.

Figure 1 shows the impedance of the micro-holes over the panel surface. As shown in [15,16], the real and imaginary parts of the micro-hole impedance are given by

$$Z_{M,R} = \frac{\rho_a c_a}{\sigma}\left(0.147\frac{h}{d^2}\right)\left(\sqrt{9+\frac{100d^2f}{32}}+1.768\sqrt{f}\frac{d^2}{h}\right), \tag{35}$$

$$Z_{M,I} = \frac{\rho_a c_a}{\sigma}1.847fh\left(1+\frac{1}{\sqrt{9+50d^2f}}+0.85\frac{d}{h}\right), \tag{36}$$

where f =ω/(2π), h is the panel thickness, and d is the perforation diameter. σ is the perforation ratio.

Finally, according to the electro-acoustic analogy adopted in [16], the total impedance and acoustic absorption of the micro-perforated panel backed by a cavity are given by

$$Z_{total} = Z_{cav} + \frac{Z_M Z_P}{Z_M + Z_P}, \tag{37}$$

$$\alpha_{total} = \frac{4\mathrm{RE}(Z_{total})}{(1+\mathrm{RE}(Z_{total}))^2 + (\mathrm{IM}(Z_{total}))^2} \tag{38}$$

where Z_{cav} is the cavity impedance and given by $-j\rho_a c_a \omega \cot(\omega D/c_a)$; D is the cavity depth.

3. Results and discussion

Figure 2 compares the results obtained from the numerical integration method [17] and the proposed method. The material and physical properties of the curved metal panel are set as follows: Young's modulus E = 71 × 10^9 N/m^2, Poisson's ratio ν = 0.3, mass density ρ_p = 2700 kg/m^3, panel length a = 300 mm, panel width b = 100 mm, panel thickness h = 2 mm, and damping ratio ξ = 0.01. In Figure 2, the displacement amplitude is plotted against the excitation frequency. In general, the two sets of results are in reasonable agreement with each other. A detectable discrepancy is found at the nonlinear resonant peak around 100 to 110 Hz. Here, the peak frequencies from the two methods are somewhat different because the phase angle in the proposed solution form, which represents the damping and thus affects the peak value, is different from that in [17]. Tables 1–3 show the

convergence results for various excitation levels and excitation frequencies. In these cases, the maximum vibration amplitude/panel thickness ratio is over 1.4, so these cases can be classified as highly nonlinear. It can be seen that the two-mode and two-harmonic-term approach is accurate enough for the numerical cases. Some other direct space–time discretization solution methods (e.g., the structure-preserving algorithm in [1,2]) may be suitable for solving this nonlinear problem and can be considered in further work.

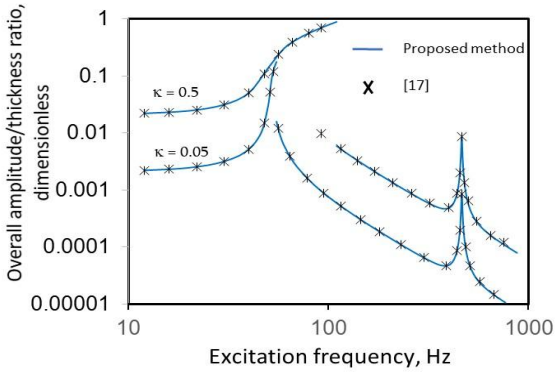

Figure 2. Comparison between the results obtained from the proposed method and numerical simulation method.
Note: The panel amplitudes are normalized as 100%.

Table 1. Convergence result (2 panel modes; A_o=0; ξ=0.01; and ω = 50 Hz).

	κ = 0.05	= 5	= 30
1 harmonic term	99.98%	97.22%	86.17%
2 harmonic terms	100.00%	99.93%	98.73%
3 harmonic terms	100.00%*	100.00%*	100.00%*

Note: The panel amplitudes are normalized as 100%.

Table 2. Convergence result (2 panel modes; A_o=0; ξ=0.01; and ω = 100 Hz).

	κ = 0.05	= 5	= 30
1 harmonic term	94.21%	94.07%	93.07%
2 harmonic terms	97.26%	97.45%	97.93%
3 harmonic terms	100.00%*	100.00%*	100.00%*

Note: The panel amplitudes are normalized as 100%.

Table 3. Convergence result (2 harmonic terms; A_o=0; ξ=0.01; and ω = 400 Hz).

	κ = 0.05	= 5	= 30
1 mode approach	73.15%	73.16%	73.41%
2 mode approach	99.99%	99.99%	99.99%
3 mode approach	100.00%*	100.00%*	100.00%*

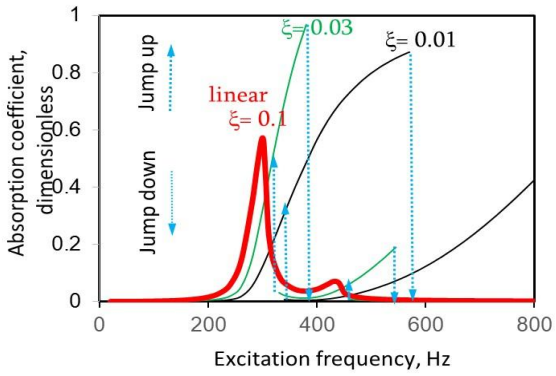

Figure 3. Absorption coefficient versus excitation frequency for various excitation levels (κ = 2, 10, 30, from small to large excitations).

Figures 3 and 4 show the absorption plotted against the excitation frequency for various excitation levels and damping ratios, neglecting any perforation effect. The material and physical properties of the curved metal panel are set as follows: $E = 200 \times 10^9$ N/m^2, $\nu = 0.3$, $\rho_p = 7800$ kg/m^3, $a = 200$ mm, $b = 100$ mm, $h = 0.8$ mm, and the pre-set static middle deflection $A_o = 2$ mm. There are two peaks in each of the two figures, which are caused by the resonances of the first and second modes, respectively. Additionally, the so-called "jump" phenomenon is observed, which can be interpreted as indicating multi-solution outcomes in the real world. The governing equation is a cubic nonlinear differential equation and may have more than one solution in some frequency ranges. When a vibration response type that represents one particular solution outcome changes to another response type, this can be considered a jump phenomenon. It can be found that a stronger excitation or smaller damping ratio can result in a wider resonant or absorption bandwidth and higher jump frequency, particularly for "jump-down" cases. If the damping is too high or the excitation is too weak, there is no nonlinear behavior. The peaks due to the first-mode resonance are higher than that of the second mode because of the greater modal contribution. Generally, the higher the damping ratio is, the narrower the absorption bandwidth is. In other words, to improve the absorption performance, the damping of the panel or the panel thickness or curvature should be tuned appropriately. Figures 5–7 show the sound absorption by a perforated panel backed by a cavity, plotted against the excitation frequency, for various excitation levels. The perforation absorption peak frequency is around 140 Hz. There is a large trough in each figure, which is caused by the cavity anti-resonance around 480 Hz. The vibrating-panel effect due to the second mode is insignificant relative to the perforation effect. Generally, the absorption bandwidths in the jump-down cases are wider than those in the jump-up cases. Note that there is no jump phenomenon in Figure 7 because the excitation level is too low. It can be seen that in the case of $\kappa = 30$, the absorption bandwidths of 300 to 400 Hz and 600 to 800 Hz are wider than those in the other two cases. Figures 8–10 show three cases, in which the first-mode resonant frequencies are tuned to 84, 148, and 202 Hz, respectively. There is a trough near the first-mode resonant frequency in each case. The air particle movement around the perforation holes on the panel causes the sound absorption. However, when the panel vibrates in the same direction as the air particle movement, the relative air particle movement around the perforation decreases. Therefore, this negative vibrational effect offsets the positive perforation effect. This implies that the resonant vibration effect can impair the absorption performance if the panel resonant frequency is inappropriately set. From these figures, it can be seen that the nonlinear

vibration effect generally enhances the absorption performance of a panel if the panel configuration is appropriately tuned.

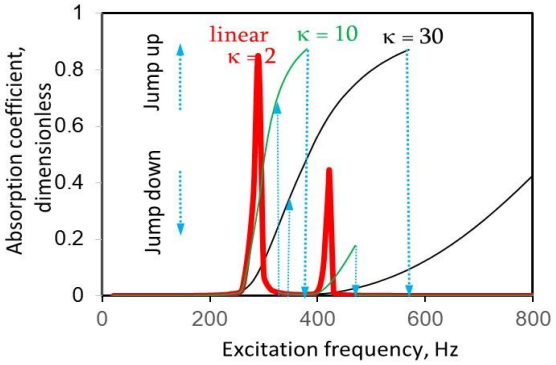

Figure 4. Absorption coefficient versus excitation frequency for various damping ratios (ξ = 0.01, 0.03, 0.1, from small to large damping ratios).

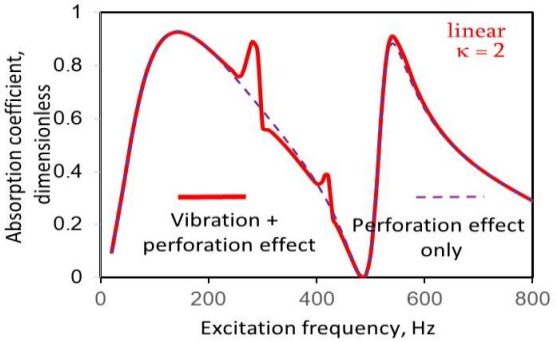

Figure 5. Absorption coefficient versus excitation frequency for the cases with/without vibration effect (excitation level, κ=2, small excitation).

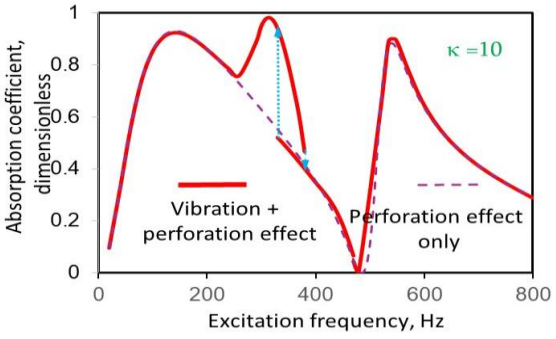

Figure 6. Absorption coefficient versus excitation frequency for the cases with/without vibration effect (excitation level, κ=10, moderate excitation).

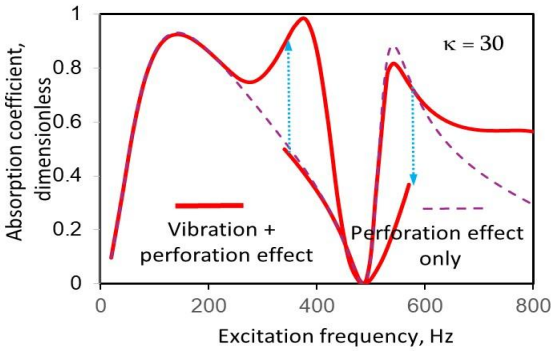

Figure 7. Absorption coefficient versus excitation frequency for the cases with/without vibration effect (excitation level, κ=30, large excitation).

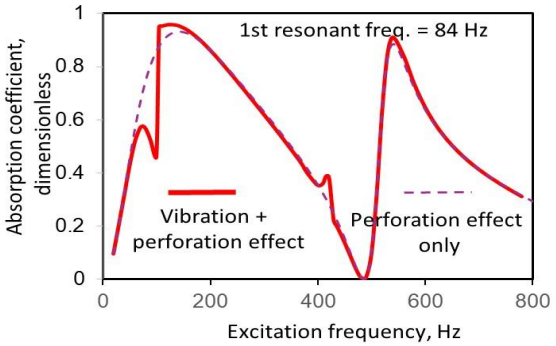

Figure 8. Absorption coefficient versus excitation frequency for the cases with/without vibration effect (1st resonant frequency = 84 Hz).

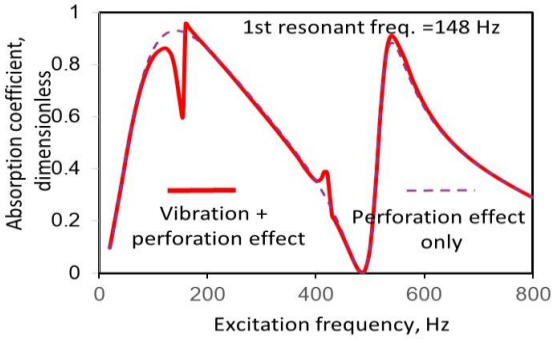

Figure 9. Absorption coefficient versus excitation frequency for the cases with/without vibration effect (1st resonant frequency = 148 Hz).

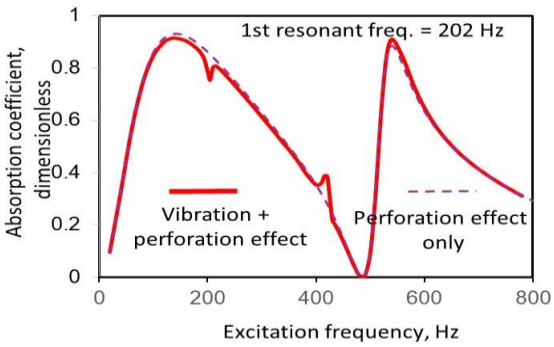

Figure 10. Absorption coefficient versus excitation frequency for the cases with/without vibration effect (1st resonant frequency = 202 Hz).

4. Conclusions

In this paper, we have presented the absorption analysis of nonlinear multi-mode panel absorber using a phase angle elimination method, which is newly applied to this nonlinear structural acoustic problem. The nonlinear modal formulation is developed from the partial governing equations, which represent the large-amplitude structural vibration of a curved panel absorber. The results obtained from the proposed solution method and numerical method are generally in good agreement. The effects of excitation magnitude, pre-set static deflection, and damping ratio are investigated. It can be concluded that: 1) A stronger excitation or smaller damping ratio can result in a wider resonant or absorption bandwidth and higher jump frequencies; 2) the higher the damping ratio is, the lower the absorption peak is; and 3) the panel resonant frequency can be increased by pre-setting the initial deflection profile, ensuring that the resonant vibration has a positive effect on the absorption bandwidth. However, the panel resonant vibration effect can worsen the absorption performance if the panel resonant frequency is set near or below the perforation absorption peak frequency.

Author contributions

Kongzheng Liang: Conceptualization, Visualization, Writing-original draft; Di Zeng: Methodology, Validation, Writing-original draft; Yiuyin Lee: Conceptualization, Methodology, Investigation, Validation, Writing–review & editing; Zongxian Wang: Writing-original draft, Writing–review & editing, visualization. All authors have read and approved the final version of the manuscript for publication.

Use of Generative-AI tools declaration

The authors declare they have not used Artificial Intelligence (AI) tools in the creation of this article.

Acknowledgments

The APC was supported by iCare Technology (HK) Co. Ltd.

Conflict of interests

The authors declare that they have no competing interests in this paper.

References

1. W. P. Hu, X. Y. Yan, Z. Q. Han, Z. Y. Wang, Z. C. Deng, Modeling and dynamic analysis on spar-type floating offshore wind turbines system via structure-preserving iterative method, *Appl. Math. Modell.*, **151** (2026), 116562. https://doi.org/10.1016/j.apm.2025.116562
2. X. J. Xi, W. P. Hu, J. W. Yan, F. Wu, C. Z. Zhang, Structure-preserving analysis on hub-cracked beam with hollow tapered cross-section, *Mech. Syst. Signal Proc.*, **240** (2025), 113374. https://doi.org/10.1016/j.ymssp.2025.113374
3. W. P. Hu, Z. Q. Han, F. Wu, J. W. Yan, Z. C. Deng, Coupling dynamic behaviors of flexible thin-walled tapered hub-beam with a tip mass, *J. Vib. Eng. Technol.*, **13** (2025), 447. https://doi.org/10.1007/s42417-025-01933-3
4. X. E. Kan, Y. J. Lu, F. Zhang, W. P. Hu, Approximate symplectic approach for mistuned bladed disk dynamic problem, *Mech. Syst. Signal Proc.*, **208** (2024), 110960. https://doi.org/10.1016/j.ymssp.2023.110960
5. S. Chen, Y. C. Fan, Q. H. Fu, H. J. Wu, Y. B. Jin, J. B. Zheng, et al., A review of tunable acoustic metamaterials, *Appl. Sci.-Basel*, **8** (2018), 1480. https://doi.org/10.3390/app8091480
6. R. Pandey, K. K. Shukla, A. Jain, Thermoelastic stability analysis of laminated composite plates: An analytical approach, *Commun. Nonlinear Sci. Numer. Simul.*, **14** (2009), 1679–1699. https://doi.org/10.1016/j.cnsns.2008.02.010
7. Y. Q. Li, W. K. Yao, Double-mode modeling of nonlinear flexural vibration analysis for a symmetric rectangular honeycomb sandwich thin panel by the homotopy analysis method, *Math. Methods Appl. Sci.*, **44** (2021), 7–26. https://doi.org/10.1002/mma.6703
8. M. A. Shahmohammadi, S. M. Mirfatah, H. Salehipour, O. Civalek, On nonlinear forced vibration of micro scaled panels, *Int. J. Eng. Sci.*, **182** (2023), 103774. https://doi.org/10.1016/j.ijengsci.2022.103774
9. M. Y. Zheng, H. Y. Shen, H. B. Xie, Broadband sound absorption under oblique incidence based on ultra-micro-perforated panel absorber, *J. Phys. D-Appl. Phys.*, **58** (2025), 235302. https://doi.org/10.1088/1361-6463/add7e6
10. Y. Y. Lee, E. W. M. Lee, C. F. Ng, Sound absorption of a finite flexible micro-perforated panel backed by an air cavity, *J. Sound Vib.*, **287** (2005), 227–243. https://doi.org/10.1016/j.jsv.2004.11.024
11. Y. Y. Lee, Analytic formulation for the sound absorption of a panel absorber under the effects of microperforation, air pumping, linear vibration and nonlinear vibration, *Abstr. Appl. Anal.*, **2014** (2014), 906506. https://doi.org/10.1155/2014/906506
12. Y. Y. Lee, J. L. Huang, C. K. Hui, C. F. Ng, Sound absorption of a quadratic and cubic nonlinearly vibrating curved panel absorber, *Appl. Math. Modell.*, **36** (2012), 5574–5588. https://doi.org/10.1016/j.apm.2012.01.006
13. W. P. Hu, Z. C. Deng, T. T. Yin, Almost structure-preserving analysis for weakly linear damping nonlinear Schrodinger equation with periodic perturbation, *Commun. Nonlinear Sci. Numer. Simul.*, **42** (2017), 298–312. https://doi.org/10.1016/j.cnsns.2016.05.024

14. J. Zhou, M. L. Xu, Z. C. Yang, Y. S. Gu, Suppression of panel flutter response in supersonic airflow using a nonlinear vibration absorber, *Int. J. Non-linear Mech.*, **133** (2021), 103714. https://doi.org/10.1016/j.ijnonlinmec.2021.103714
15. D. Maa, Microperforated-panel wideband absorbers, *Noise Control Eng. J.*, **29** (1987), 77–84. https://doi.org/10.3397/1.2827694
16. D. Maa, Potential of microperforated panel absorber, *J. Acoust. Soc. Am.*, **104** (1988), 2861–2866. https://doi.org/10.1121/1.423870
17. Y. Y. Lee, Q. S. Li, A. Y. T. Leung, R. K. L Su, The jump phenomenon effect on the sound absorption of a nonlinear panel absorber and sound transmission loss of a nonlinear panel backed by a cavity, *Nonlinear Dyn.*, **69** (2012), 99–116. https://doi.org/10.1007/s11071-011-0249-2

AIMS Press